Available online at www.sciencedirect.com

ScienceDirect

www.elsevier.com/locate/jes

JES JOURNAL OF ENVIRONMENTAL SCIENCES

www.jesc.ac.cn

Heterogeneous uptake of NO_2 by sodium acetate droplets and secondary nitrite aerosol formation

Wen-Xiu Pei[1], *Shuai-Shuai Ma*[2], *Zhe Chen*[1], *Yue Zhu*[1], *Shu-Feng Pang*[1,*], *Yun-Hong Zhang*[1,*]

[1] *School of Chemistry and Chemical Engineering, Beijing Institute of Technology, Beijing 100081, China*
[2] *College of Chemistry and Material Engineering, Quzhou University, Quzhou 324000, China*

ARTICLE INFO

Article history:
Received 11 January 2022
Revised 25 May 2022
Accepted 25 May 2022
Available online 3 June 2022

Keywords:
Heterogeneous uptake
NaAc droplets
Nitrite
Uptake coefficient

ABSTRACT

The high NO_3^- concentration in fine particulate matters ($PM_{2.5}$) during heavy haze events has attracted much attention, but the formation mechanism of nitrates remains largely uncertain, especially concerning heterogeneous uptake of NO_X by aqueous phase. In this work, the heterogeneous uptake of NO_2 by sodium acetate (NaAc) droplets with different NO_2 concentrations and relative humidity (RH) conditions is investigated by microscopic Fourier transform infrared spectrometer (micro-FTIR). The IR feature changes of aqueous droplets indicate the acetate depletion and nitrite formation in humid environment. This implies that acetate droplets can provide the alkaline aqueous circumstances caused by acetate hydrolysis and acetic acid (HAc) volatilization for nitrite formation during the NO_2 heterogeneous uptake. Meanwhile, the nitrite formation will exhibit a pH neutralizing effect on acetate hydrolysis, further facilitating HAc volatilization and acetate depletion. The heterogeneous uptake coefficient increases from 5.2×10^{-6} to 1.27×10^{-5} as RH decreases from 90% to 60% due to the enhanced HAc volatilization. Furthermore, no obvious change in uptake coefficient with different NO_2 concentrations is observed. This work may provide a new pathway for atmospheric nitrogen cycling and secondary nitrite aerosol formation.

Introduction

Recent field measurements have introduced the increased ratio of NO_2 to SO_2 (Zhou et al., 2021) and the increased conversion efficiency of NO_X to HNO_3 due to more OH radicals and O_3 (Fu et al., 2020), causing the higher concentration of NO_3^- than SO_4^{2-} in $PM_{2.5}$ during heavy haze events in China (Li et al., 2021; Sun et al., 2019; Xu et al., 2019). Moreover, atmospheric organic matters (OM) also greatly contribute to mass concentration of $PM_{2.5}$ (Chen et al., 2015; Sun et al., 2019; Tian et al., 2016). All of these indicate that in recent years, fine particle explosive growth during heavy haze episodes in China may be dominated mainly by the formation of nitrate and OM instead of sulfate.

The formation of nitrogenous aerosols of atmospheric significance have been extensively studied in laboratory and field measurements, mainly focusing on atmospheric heterogeneous chemistry, photochemical reactions, as well as multiphase redox processes. In other words, atmospheric nitrogen oxides can be converted to nitrite and nitrate aerosols via various redox pathways, i.e., photooxidation by OH radicals and O_3 in the gas phase (Chen et al., 2020; Lu et al., 2019), heterogeneous reactions on highly reactive surfaces

* Corresponding authors.
E-mails: sfpang@bit.edu.cn (S.-F. Pang), yhz@bit.edu.cn (Y.-H. Zhang).

https://doi.org/10.1016/j.jes.2022.05.048
1001-0742/

of sea salt and mineral dust aerosols (Gibson et al., 2006; Wu et al., 2020; Ye et al., 2010), photochemical reactions on photoactive mineral dust and soot surfaces (Chen et al., 2012; Fang et al., 2021; Wang et al., 2021), and aqueous redox processes in humid circumstance (Chen et al., 2004; Liu et al., 2015; Tan et al., 2017). Due to the complex reactive nitrogen chemistry, many endeavors about the NO_X heterogeneous uptake have been made to ascertain the formation mechanism of nitrogenous aerosols (Li et al., 2010; Liu et al., 2017; Yu et al., 2021). Hoffman et al. (2003) observed the heterogeneous reaction of N_2O_5 with sea salt causing $NaNO_3$ formation, and the heterogeneous uptake coefficient (γ) was determined to be $(2.9 \pm 1.7) \times 10^{-3}$ in single layer particle studies. Yabushita et al. (2009) investigated the uptake of NO_2 by alkaline NaCl droplets with an electrospray mass spectrometer. The results implied that OH^- is able to catalyze the disproportionation of NO_2(g) into NO_2^- and NO_3^-. Jia et al. (2021) investigated the formation of nitrate on $CaCO_3$ particles at different RHs. They found that the elevated RH (20% - 80%) was markedly favorable for the heterogeneous reactivity of $CaCO_3$ toward NO_2 compared with that under dry condition, owing to the water uptake by formed nitrate on $CaCO_3$ surface. Likewise, Tan et al. (2016) studied the heterogeneous reaction of NO_2 with $(NH_4)_2SO_4$, $CaCO_3$ and mixed $(NH_4)_2SO_4/CaCO_3$ particles. The results showed that heterogeneous uptake of NO_2 did not occur on $(NH_4)_2SO_4$ particles, but it occurred on $CaCO_3$ surface causing $Ca(NO_3)_2$ formation under both dry and wet conditions. The mixing of $(NH_4)_2SO_4$ into $CaCO_3$ particles exhibited negligible effects on NO_2 uptake under dry condition. Whereas under the wet condition, the chemical interaction between $(NH_4)_2SO_4$ and $Ca(NO_3)_2$ and the coagulation of $(NH_4)_2SO_4$ with $CaCO_3$ respectively facilitated and inhibited the nitrate formation. Therefore, the ambient RH may be a key factor dictating the heterogeneous reaction kinetics of NO_X.

For nitrite aerosol formation, Li et al. (2010) observed the production of nitrite under wet condition during the reaction of NO_2 on $CaCO_3$ surface. At low RH, only nitrate was formed due to interaction of NO_2 with surface –OH, which came from dissociation of surface adsorbed water via oxygen vacancy. While at RH $>$ 52%, the reaction of NO_2 with condensed water was dominant to produce nitrous acid (HONO) and HNO_3. Wu et al. (2013) studied the effect of temperature on the heterogeneous reaction kinetics of NO_2 on γ-Al_2O_3 surface at dry conditions. Nitrite as an intermediate product was converted to bidentate nitrate at temperatures between 250 and 318 K. As the temperature decreased, the conversion rate increased. Besides, Wang et al. (2021) investigated the influence of irradiation intensity on product distribution and kinetics of photochemical reaction of NO_2 on mineral dust particles. They found that the proportion of nitrite formed on Al_2O_3 and TiO_2 surfaces decreased sharply under light irradiation compared with that at dark conditions, owing to the faster photolysis of nitrite than nitrate and the facilitating effect on NO_2 oxidation by OH radicals. The heterogeneous chemistry and photochemical reactions of NO_2 with sea salt, mineral dust and soot particles has been extensively reported, but until now, little is known about the heterogeneous uptake of NO_2 by aqueous alkaline droplets.

Sea salt aerosols can be chemically processed by water-soluble carboxylic acids from anthropogenic sources offshore, resulting in chloride depletion and carboxylic acid salt formation (Kerminen et al., 1998; Laskin et al., 2012). As far as we know, acetic acid is the most abundant monocarboxylic acid in the troposphere, with a gas phase concentration about 0.05-16 ppb (Hou et al., 2016). Once acetic acid is released into the atmosphere, especially in coastal areas, it reacts with sea salt aerosols, such as NaCl, to form sodium acetate. There is data showing that the concentration of carboxylate is 1352.8 ± 680.9 ng/m^3 and 1374.1 ± 560.2 ng/m^3 in the urban and industrial areas of Southeast Asia, and acetate accounts for 26.87% and 34.25%, respectively (Tsai et al., 2013). The physicochemical properties of acetates have been previously explored by a number of studies (Gao et al., 2018; Lv et al., 2018; Peng and Chan, 2001; Wu et al., 2011). Additionally, during the heavy haze, another critical characteristic of fine particle explosive growth is high RH, expect for high NO_3^- and OM concentrations (Sun et al., 2019). Accordingly, the acetate component in $PM_{2.5}$ may exist in aqueous solution phase in most conditions during the haze due to the relatively low DRH, i.e., 48% DRH at 295.8 K for sodium acetate particles (Gao et al., 2018). This will post a key question that whether the acetate solution phase can affect the heterogeneous uptake of NO_X and contribute to high NO_3^- concentration. Also, how the high RH and NO_X concentration influence the heterogeneous redox process?

In this work, the heterogeneous uptake of NO_2 by atmospherically relevant sodium acetate droplets under different RHs and NO_2 concentrations is investigated using micro-FTIR combined with a gas-flow system. Analyzing of the IR features of aqueous droplets reveals the formation of nitrite in aqueous media accompanied by evaporation of acetic acid. Furthermore, the formation mechanism of nitrite and the effects of ambient RH and NO_2 concentration are explored. To our knowledge, detection of the heterogeneous reaction of NO_2 with alkaline solution droplet causing secondary nitrite formation by FTIR is first introduced herein.

1. Materials and methods

1.1. *Sample preparation*

NaAc (99.0% purity) and $NaNO_2$ (99.0% purity) were purchased from Sinopharm Chemical Reagent Co., Ltd and used without further purification. Solutions of NaAc and $NaNO_2$ were prepared by dissolving their solids into ultrapure water (18.2 MΩ cm). Aerosols were generated by spraying solution onto the ZnSe windows with a syringe and the droplet diameter is about 100 μm. Zero air (99.999%, 22% O_2 and 78% N_2), used to simulated the ambient air, and NO_2 (500 ppm mixed with N_2), as a reactant gas, were supplied by Beijing Huatongjingke Gas Chemical Co., Ltd.

1.2. *Gas supply system*

The gas supply system consisted of three lines. The first line transported NO_2 as the gaseous reactant. The second and third line supplied dry air and humid air (water saturated air, produced by flowing a bubbler containing ultrapure water), which can dilute the NO_2 gas to desired concentrations and

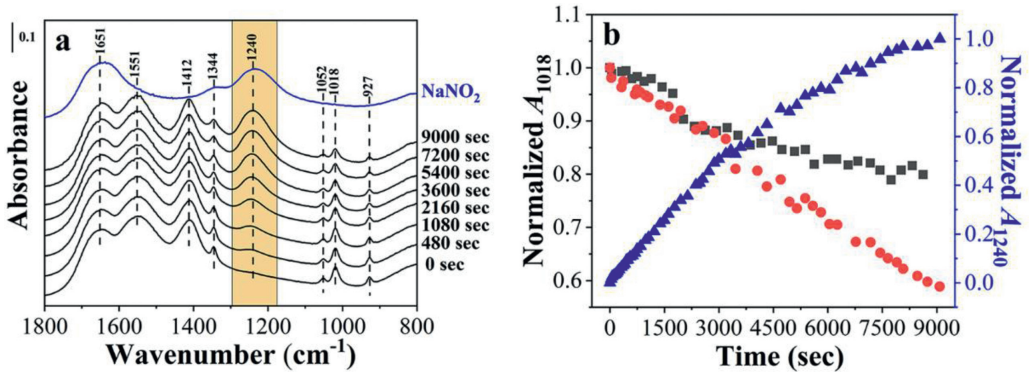

Fig. 1 – (a) IR spectra of NaAc droplets exposed to 50 ppm NO_2 mixed with air under constant 80% RH at different exposure time. The blue curve represents the reference spectrum of pure $NaNO_2$ droplets measured by micro-FTIR. (b) Normalized integrated absorbance of 1018 cm^{-1} band (A_{1018}, represented by red circles) assigned to acetate and 1240 cm^{-1} band (A_{1240}, represented by blue triangles) assigned to nitrite as a function of exposure time when the NaAc droplet is exposed to NO_2 mixed with air. The black squares indicate the A_{1018} values when the NaAc droplet is exposed to air only. (For interpretation of the references to color in this figure legend, the reader is referred to the web version of this article.)

the RH in sample cell was controlled by adjusting the flow ratio of dry air and humid air. The total gas-flow rate was controlled to be about 400 mL/min by three mass flow controllers (Alicat) installed upstream. The NO_2 concentration and ambient RH in sample chamber were detected by a NO_2 monitor and a hygrometer (Center 313) installed downstream, respectively.

1.3. *Experimental instrument*

The experimental setup was constructed by the micro-FTIR spectrometer (Nicolet IN10^{TM}) combined with a gas supply system in Fig. S1. The experimental instrument has been described in details elsewhere (He et al., 2017; Lian et al., 2020), and thus we give a brief introduction here. The micro-FTIR spectrometer was equipped with a liquid-nitrogen-cooled Mercury Cadmium Telluride (MCT) detector. Both the infrared light and visible light from the bottom of micro-FTIR passed through the sample chamber, and then entered into the MCT and visible light detectors, respectively. Based on this, the IR spectra and particle morphology of sample droplets could be synchronously detected. During the measurement, the IR spectra were automatically collected by 64 scans with a resolution of 4 cm^{-1} in the spectral range of 800–4000 cm^{-1}. All the measurements were performed more than three times at 23–26 °C.

2. Results and discussion

2.1. *Heterogeneous uptake of NO_2 by NaAc droplets and nitrite formation mechanism*

The IR spectra of NaAc droplets exposed to 50 ppm NO_2 under constant 80% RH at different exposure time are shown in Fig. 1a. At $t = 0$ sec, the bands at 1551 cm^{-1} and 1412 cm^{-1} are assigned to $-COO^-$ asymmetric and symmetric stretch modes of acetate, respectively (Noma et al., 1991), indicating the free CH_3-COO^- ions in the NaAc droplet. The bands at 1344 cm^{-1}, 1052 cm^{-1}, 1018 cm^{-1} are attributed to symmetric stretch, out-of-plane rocking, and in-plane rocking vibrations of $-CH_3$, respectively (Wilmshurst, 1955). The C-C stretch mode is located at 927 cm^{-1} (Kemper, 1990). Furthermore, the 1651 cm^{-1} band arises from the bending mode of liquid water molecules (Du et al., 2020; Ma et al., 2019). As NO_2 gas is introduced into the sample chamber, a new peak located at 1240 cm^{-1} appears at $t = 480$ sec. This band can be assigned to the NO_2^- asymmetric stretch vibration of $NaNO_2$ (blue curve in Fig. 1a) (Allen et al., 1994; Li et al., 2010; Liu et al., 2012), indicating the formation of nitrite within the NaAc droplet. Then, the feature band intensity increases with exposure time due to the continuous production of nitrite. Meanwhile, the feature bands assigned to acetate becomes weaker owing to the continuous consumption of acetate, which will be discussed in detail below.

For a better illustration of chemical composition evolution of NaAc droplet exposed to NO_2, the normalized integrated absorbance of 1018 cm^{-1} band (A_{1018}) assigned to acetate and 1240 cm^{-1} band (A_{1240}) assigned to nitrite as a function of exposure time are determined and shown in Fig. 1b. Note that the quantitative data of NaAc droplet exposed to air only are involved for comparison. As indicated by our previous work, the hydrolysis of $Mg(Ac)_2$, driven by acetic acid liberation, would proceed in aqueous droplets at high RH, leading to acetate depletion (Wang et al., 2018). Herein, when the NaAc droplet is exposed to air only, about 18% acetate is depleted at $t = 9000$ sec via NaAc hydrolysis, as shown in Fig. 1b. Corresponding IR spectra are shown in Fig. S2 in the Supplementary Material. The exposure to NO_2 mixed with air will cause additional ~ 20% acetate depletion at $t = 9000$ sec due to the continuous formation of nitrite, represented by the changes in integrated absorbance of 1240 cm^{-1} band (blue triangles in Fig. 1b). The mechanism will be discussed detailed as follows.

$$CH_3COONa(aq) \rightleftarrows CH_3COO^-(aq) + Na^+(aq) \quad (R1)$$

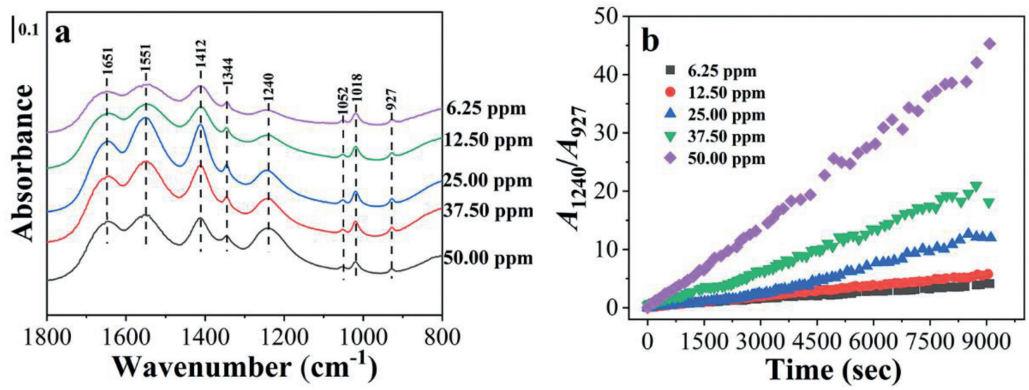

Fig. 2 – (a) IR spectra of NaAc droplets at t = 9000 sec when the droplets are exposed to NO_2 with different concentrations under constant 80% RH, and (b) corresponding A_{1240}/A_{927} values as a function of exposure time.

$$CH_3COO^-(aq) + H_2O \rightleftarrows CH_3COOH(aq) + OH^-(aq) \quad (R2)$$

$$NO_2\ (g) + OH^-\ (aq) \rightarrow NO_2^-\ (aq) + \frac{1}{2}H_2O + \frac{1}{4}O_2\ (g) \quad (R3)$$

$$CH_3COOH(aq) \rightleftarrows CH_3COOH(g)\uparrow \quad (R4)$$

Firstly, the acetate ions derived from ionization of NaAc will hydrolyze in aqueous media to form acetic acid and OH^-. Then, NO_2 can be reduced to NO_2^- by OH^- along with the production of O_2. This process has been introduced by Chen et al. (2004) for the conversion of NO_2 to NO_2^- in NaOH alkaline solution. While to our knowledge, this conversion process is proposed for the first time in aerosol systems herein. It should be noted that the interaction between NO_2 and H_2O could cause formation of both nitric acid and nitrous acid (Liu et al., 2015; Tan et al., 2017). Therefore, the absence of nitrate in this work implies that the reaction (R3) may dominate in heterogeneous uptake of NO_2 by NaAc droplet, owing to the pH dependence of formation mechanism of nitrogenous species (Chen et al., 2004). In addition, the reaction (R3) will exhibit a pH neutralizing effect on acetate hydrolysis, which increases the acetate depletion and further promotes HAc partition into the gas phase. More importantly, the formed nitrite can be further oxidized to form nitrate by dissolved oxidants (H_2O_2, O_3), or be acidized to produce HNO_2 or gaseous HONO in the atmosphere.

2.2. *Effect of NO_2 concentration on heterogeneous reaction kinetics*

To gain insights into the heterogeneous reaction kinetics of NO_2 with the NaAc droplet, the effects of different NO_2 concentrations and ambient RH on the heterogeneous reaction are explored. Fig. 2a shows the IR spectra of NaAc droplets exposed to NO_2 with different concentrations at t = 9000 sec under constant 80% RH. It is clear that the 1240 cm^{-1} band assigned to nitrite becomes stronger with increasing NO_2 concentration. For further comparison, corresponding integrated absorbance ratio of 1240 cm^{-1} band (NO_2^-) to 927 cm^{-1} band (C–C), i.e., A_{1240}/A_{927} values as a function of exposure time are determined and shown in Fig. 2b. Note that the A_{1240}/A_{927} is the representative of the relative amount of formed nitrite to remaining acetate, similar to the treatment from Yang et al. (2020). As the NO_2 concentration rises from 6.25 ppm to 50.00 ppm, the formation rates and final relative amount of nitrite greatly increase. Additionally, the A_{1240} values show an almost linear increase with exposure time (seen Fig. S3), potentially implying that the heterogeneous uptake of NO_2 by NaAc droplets obeys to the pseudo-zero-order reaction, due to the almost unchanged reactant concentration caused by continuous HAc volatilization and NaAc hydrolysis (Yang et al., 2020). It should be noted that the formation rates of nitrite with 50.00 ppm NO_2 concentration show a slight decrease after about 6000 sec, which can be attributed to the insufficient acetate due to the large amounts of nitrite formation.

The formation rate of nitrite, d{NO_2^-}/dt (ions/(cm^3•sec)), defined as the amount of nitrite ions formed within the NaAc droplet per unit volume per unit time during the reaction. In present work, the IR spectra of NaAc aerosols exposing onto NO_2 gas with various concentrations were measured, and the integrated area of 1240 cm^{-1} band as a function of exposing time were plotted shown in Fig. S3. Then the calibration curve of the integrated areas of the 1240 cm^{-1} band dependent upon the nitrite ions concentration was built first by measuring IR spectra of a series of sodium nitrite solution with different known concentrations seen in Fig. S4. From Fig. S4, the linear fitting equation $A = 11.8\ c + 0.31$ can be acquired, which was applied to the intensity of 1240 cm^{-1} band of studied aerosols in Fig. S3. So the nitrite concentration evolution with exposing time under different NO_2 concentration can be gained, from which d{NO_2^-}/dt (ions/(cm^3•sec)) was known. The treatment method is similar to that reported by Lian et al. (2020) and Liu et al. (2017). And the nitrite formation rates at varied NO_2 gas concentrations are shown in Fig. 3. Obviously, a positive correlation between the nitrite formation rates and NO_2 concentration is presented.

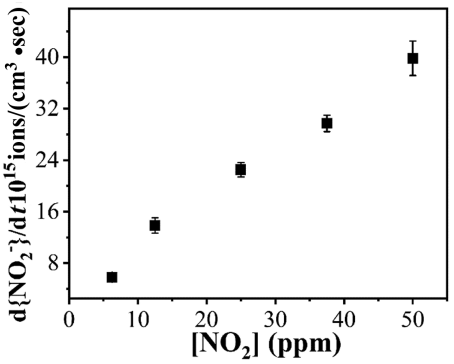

Fig. 3 – The formation rates of nitrite, $d\{NO_2^-\}/dt$ (ions/(cm3·sec), as a function of NO_2 concentration under constant 80% RH.

2.3. *Effect of ambient RH on heterogeneous reaction kinetics*

Figure 4a shows the IR spectra of NaAc droplets exposed to NO_2 with the fixed concentration of 6.25 ppm at $t = 9000$ sec under different RH conditions. Firstly, the NaAc droplet can be effloresced around 41% RH, judged from the feature band changes shown in Fig. 4a (red curve). Specifically, the 1412 cm^{-1} band is split into three shoulder bands at 1450, 1425 and 1412 cm^{-1}, and the 1551, 1052 and 927 cm^{-1} bands shift to 1565, 1041 and 921 cm^{-1}, consistent with the observation by Gao et al. (2018). Thus the NaAc droplet has been effloresced completely at ~ 3% RH (blue curve in Fig. 4a). Meanwhile, no obvious feature band of NO_2^- is observed after 9000 sec exposure, indicating the prerequisite of an aqueous media for the heterogeneous reaction. Then, the final peak intensity of 1240 cm^{-1} band at constant 60% RH is markedly higher than that at 90% RH. Further, the A_{1240}/A_{927} values during NO_2 exposure periods under four different RHs, i.e., 60%, 70%, 80% and 90%, are determined and shown in Fig. 4b. As seen, the formation rates and final relative amount of nitrite significantly increase with lower RH. This can be explained by the enhanced volatilization of HAc at lower RH. The driving out of volatile species such as HAc from aqueous droplets can be described by Maxwell steady-state diffusive mass transfer equation (Cai et al., 2014; Chen et al., 2021; Ray et al., 1979), which can be determined as

$$-\frac{dm}{dt} = \frac{4\pi rMD}{RT}(p_\infty - p_r) \quad (1)$$

where m denotes the HAc mass within the droplet (g) and t denotes the evaporation time (sec); M and D respectively denote the molecular weight of HAc (g/mol) and its diffusion coefficient in air (m^2/sec); r is the droplet radius (m); R and T are the ideal gas constant (J/(mol·K)) and temperature (K), respectively; p_∞ and p_r denote the HAc partial pressure (Pa) at infinite distance and droplet surface, respectively. Based on this, the dm/dt (g/sec), indicative of evaporation rate of HAc, is suggested to be positively related to p_r assuming $p_\infty = 0$. Therefore, the reduction in RH will cause the enrichment of HAc within the droplet, further leading to higher HAc partial pressure at droplet surface due to the Raoult effect, which ultimately causes faster HAc evaporation at lower RH. In addition, the increase in OH^- concentration due to the water release may be another cause for the facilitating effect of lower RH on the heterogeneous reaction. Likewise, high pH levels would cause more SO_2 to dissolve into the aerosol liquid water, increasing the rate at which SO_2 was converted to sulfate (Cheng et al., 2016). Routinely, the formation rates of nitrite as a function of RH are determined and shown in Fig. 5. As RH decreases from 90% to 60%, the rate significantly increases from 4.52×10^{15} to 11.0×10^{15} ions/(cm^3•sec).

2.4. *Reactive uptake coefficient measurements*

The reactive uptake coefficient, γ, characterizing the reaction efficiency of NO_2 in atmospheric particles, was defined as the ratio of reactive collision rate to total collision rate, and can be determined by He et al. (2021), Jia et al. (2021), Li et al. (2010), Li et al. (2020).

$$\gamma = \frac{d\{NO_2^-\}/dt}{Z} \quad (2)$$

$$Z = \frac{1}{4}\bar{c}A_s[NO_2] \quad (3)$$

$$\bar{c} = \sqrt{\frac{8RT}{\pi M_{NO_2}}} \quad (4)$$

where, $d\{NO_2^-\}/dt$ denotes the formation rate of nitrite within NaAc droplets (ions/(cm^3•sec)); Z is the rate of surface collisions per unit time (ions/(cm^3•sec)); $\bar{c}$ is the mean velocity of NO_2 in the gas phase (cm•/sec); A_s is the specific surface area of the NaAc single droplet (cm^{-1}); $[NO_2]$ represents the concentration of NO_2 molecules (molecule/cm^3); R is the ideal gas constant ($J\cdot mol^{-1}\cdot K^{-1}$); T is the temperature during the reactions (K); M_{NO_2} is the molecular weight of NO_2 (g/mol).

In present study, the γ values with different NO_2 concentrations and ambient RH are calculated and presented in Table 1, showing ~ 10^{-6}. The uptake coefficient under 60% RH is twice as large as that at 90% RH, suggesting that the heterogeneous reaction of NO_2 within NaAc droplet can be easily affected by the RH change. Furthermore, the γ values with different NO_2 concentrations are comparable, implying that the NO_2 uptake coefficient is independent of NO_2 concentration, which agrees with the observations by Jia et al. (2021) and Li et al. (2010). Previous studies have focused on the determination of heterogeneous uptake coefficient of NO_2 on mineral dust particles such as $CaCO_3$, kaolinite, hematite, and other metal oxides (Jia et al., 2021; Liu et al., 2015; Wang et al., 2021). As shown in Table 2, the measured uptake coefficient of NO_2 with NaAc droplet in this work is comparable with the previous results for NO_2 heterogeneous uptake on mineral dust surfaces.

3. Conclusions and atmospheric significance

In this work, the heterogeneous uptake of NO_2 by NaAc droplets under different NO_2 concentrations and RH conditions is investigated by the micro-FTIR technique. The

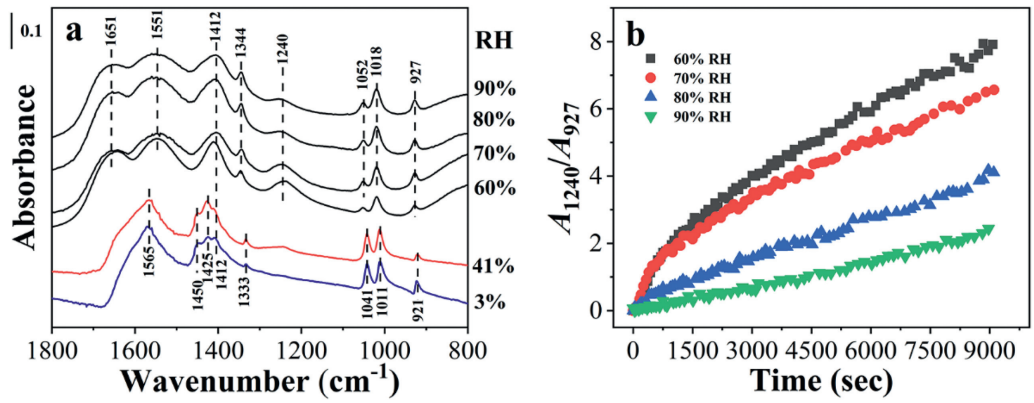

Fig. 4 – (a) IR spectra of NaAc droplets at t = 9000 sec when the droplets are exposed to NO_2 with the fixed concentration of 6.25 ppm under different RH conditions, and (b) corresponding A_{1240}/A_{927} values as a function of exposure time.

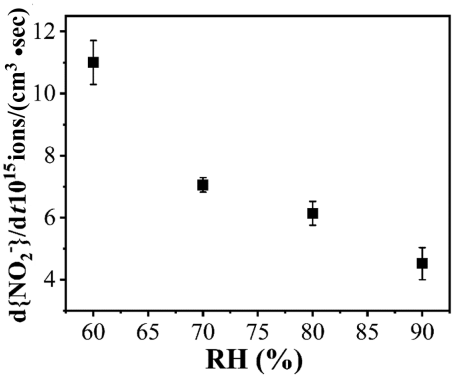

Fig. 5 – The formation rates of nitrite, $d\{NO_2^-\}/dt$ (ions/(cm^3•sec)), as a function of ambient RH with the fixed NO_2 concentration of 6.25 ppm.

Table 1 – The γ values with different RH conditions and NO_2 concentrations measured in this work.

RH (%)	γ (10^{-6})	NO_2 concentration (ppm)	γ (10^{-6})
60	12.7	50.00	5.73
70	8.13	37.50	5.70
80	7.06	25.00	6.48
90	5.20	12.50	7.97
-	-	6.25	6.70

stronger 1240 cm^{-1} band and weaker 1018 cm^{-1} band with NO_2 exposure time respectively indicate the nitrite formation and acetate depletion within NaAc droplets. The interaction mechanism is that, acetic acid volatilization will promote acetate hydrolysis and provide the alkaline aqueous circumstances for nitrite formation, which in turn exhibits a pH neutralizing effect on acetate hydrolysis and further facilitate acetate depletion. Furthermore, the formation rate of nitrite significantly increases with increasing NO_2 concentration and decreasing ambient RH, meanwhile, the NO_2 uptake coefficient is independent of NO_2 concentration, but shows considerable increase at lower RH. These results can enhance the fundamental understanding of chemical composition evolution of organic acid salts to inorganic salts during secondary aerosol formation.

The product of heterogeneous reaction between NaAc aerosols and NO_2 may have significant effects on its environmental and toxic properties in the atmosphere. Under the condition of O_3, nitrite can be further oxidized to form nitrate, which can influence pH of particles and thereby chemical reactivity. Further, nitrite is almost completely converted into HONO, caused by the acidic conditions of the aqueous phase (Villena et al., 2022), that is a source of hydroxyl (OH) radicals in the atmosphere, as well as reactive nitrogen species (NO,

Table 2 – The γ values of NO_2 on different sample particles under wet conditions.

Reference	Methods	Samples	γ (NO_2)
Wang et al. (2021)	DRIFTS	kaolinite	$\sim 7 \times 10^{-6}$
		Al_2O_3	$\sim 2.5 \times 10^{-6}$
		TiO_2	$\sim 2 \times 10^{-6}$
Liu et al. (2015)	flow tube reactor	kaolin	4.26×10^{-9}
		hematite	1.23×10^{-8}
Bartolomei et al. (2014)	flow tube reactor	paint surface	4×10^{-7}
Jia et al. (2021)	fixed-bed reactor	$CaCO_3$	$(1.21 \pm 0.45) \times 10^{-7}$
This work	micro-FTIR	NaAc droplet	5.20×10^{-6} -1.27×10^{-5}

NO_2, N_2O_3, etc.) in both the gas phase and aqueous phase. Beyond that, NO_2^-/HNO_2 plays an important role on photooxidation of vanillin in atmospheric chemistry (Pang et al., 2019). In recent study, the chemistry of nitrite is associated with freezing promoting reaction such that it can provide a highly oxidative environment for benzoic acid oxidation when it reacts with H_2O_2 under slightly acidic conditions (Ahn et al., 2022). Nitrogen dioxide (NO_2) is a ubiquitous atmospheric pollutant due to the widespread prevalence of both natural and anthropogenic sources. NaAc represents a typical weakly alkaline organic salts, which are ubiquitous in atmosphere. The present transformation mechanism from NO_2 to NO_2^- is of great significance for source of nitrite and in turn contribution to pollution and climate changes.

Declaration of Competing Interest

The authors declare that they have no known competing financial interests or personal relationships that could have appeared to influence the work reported in this article.

Acknowledgements

This work was supported by the National Natural Science Foundation of China (Nos. 91644101 and 42127806).

Appendix A Supplementary data

Supplementary material associated with this article can be found, in the online version, at doi:10.1016/j.jes.2022.05.048.

REFERENCES

Ahn, Y., Kim, J., Kim, K., 2022. Frozen hydrogen peroxide and nitrite solution: the acceleration of benzoic acid oxidation via the decreased pH in ice. Environ. Sci. Technol. 56, 2323–2333.

Allen, D.T., Palen, E.J., Haimov, M.I., Hering, S.V., Young, J.R., 1994. Fourier transform infrared spectroscopy of aerosol collected in a low pressure impactor (LPI/FTIR): method development and field calibration. Aero. Sci. Technol. 21, 325–342.

Bartolomei, V., Sorgel, M., Gligorovski, S., Alvarez, E.G., Gandolfo, A., Strekowski, R., et al., 2014. Formation of indoor nitrous acid (HONO) by light-induced NO_2 heterogeneous reactions with white wall paint. Environ. Sci. Pollut. Res. Int. 21, 9259–9269.

Cai, C., Stewart, D.J., Preston, T.C., Walker, J.S., Zhang, Y.H., Reid, J.P., 2014. A new approach to determine vapour pressures and hygroscopicities of aqueous aerosols containing semi-volatile organic compounds. Phys. Chem. Chem. Phys. 16, 3162–3172.

Chen, C., Sun, Y.L., Xu, W.Q., Du, W., Zhou, L.B., Han, T.T., et al., 2015. Characteristics and sources of submicron aerosols above the urban canopy (260 m) in Beijing, China, during the 2014 APEC summit. Atmos. Chem. Phys. 15, 12879–12895.

Chen, H.H., Nanayakkara, C.E., Grassian, V.H., 2012. Titanium dioxide photocatalysis in atmospheric chemistry. Chem. Rev. 112, 5919–5948.

Chen, X.R., Wang, H.C., Lu, K.D., Li, C.M., Zhai, T.Y., Tan, Z.F., et al., 2020. Field determination of nitrate formation pathway in winter Beijing. Environ. Sci. Technol. 54, 9243–9253.

Chen, X.Y., Okitsu, K., Takenaka, N., Bandow, H., 2004. Mechanism of the NO_2 conversion to NO_2^- in an alkaline solution. Anal. Sci. 20, 1759–1762.

Chen, Z., Liu, P., Liu, Y., Zhang, Y.H., 2021. Strong acids or bases displaced by weak acids or bases in aerosols: reactions driven by the continuous partitioning of volatile products into the gas phase. Acc. Chem. Res. 54, 3667–3678.

Cheng, Y.F., Zheng, G.J., Wei, C., Mu, Q., Zheng, B., Wang, Z.B., et al., 2016. Reactive nitrogen chemistry in aerosol water as a source of sulfate during haze events in China. Sci. Adv. 2 (12), e1601530.

Du, C.Y., Yang, H., Wang, N., Pang, S.F., Zhang, Y.-H., 2020. pH effect on the release of NH_3 from the internally mixed sodium succinate and ammonium sulfate aerosols. Atmos. Environ. 220, 117101.

Fang, X.Z., Liu, Y.Y., Li, K.J., Wang, T., Deng, Y., Feng, Y.Q., et al., 2021. Atmospheric nitrate formation through oxidation by carbonate radical. ACS Earth Space Chem. 5, 1801–1811.

Fu, X., Wang, T., Gao, J., Wang, P., Liu, Y.M., Wang, S.X., et al., 2020. Persistent heavy winter nitrate pollution driven by increased photochemical oxidants in northern China. Environ. Sci. Technol. 54, 3881–3889.

Gao, X.Y., Zhang, Y.H., Liu, Y., 2018. Temperature-dependent hygroscopic behaviors of atmospherically relevant water-soluble carboxylic acid salts studied by ATR-FTIR spectroscopy. Atmos. Environ. 191, 312–319.

Gibson, E.R., Hudson, P.K., Grassian, V.H., 2006. Physicochemical properties of nitrate aerosols: implications for the atmosphere. J. Phys. Chem. A 110, 11785–11799.

He, X., Pang, S.F., Ma, J.B., Zhang, Y.H., 2017. Influence of relative humidity on heterogeneous reactions of O_3 and O_3/SO_2 with soot particles: Potential for environmental and health effects. Atmos. Environ. 165, 198–206.

He, X., Wu, J.J., Ma, Z.C., Xi, X., Zhang, Y.H., 2021. NH_3-promoted heterogeneous reaction of SO_2 to sulfate on α-Fe_2O_3 particles with coexistence of NO_2 under different relative humidities. Atmos. Environ. 262, 118622.

Hoffman, R.C., Gebel, M.E., Fox, B.S., Finlayson-Pitts, B.J., 2003. Knudsen cell studies of the reactions of N_2O_5 and $ClONO_2$ with NaCl: development and application of a model for estimating available surface areas and corrected uptake coefficients. Phys. Chem. Chem. Phys. 5, 1780–1789.

Hou, S.Q., Tong, S.R., Zhang, Y., Tan, F., Guo, Y.C., Ge, M.F., 2016. Heterogeneous uptake of gas-phase acetic acid on the surface of alpha-Al_2O_3 particles: temperature effects. Chem. Asian J. 11, 2749–2755.

Jia, X.H., Gu, W.J., Peng, C., Li, R., Chen, L.X.D., Wang, H.L., et al., 2021. Heterogeneous reaction of $CaCO_3$ with NO_2 at different relative humidities: kinetics, mechanisms, and impacts on aerosol hygroscopicity. J. Geophys. Res. Atmos. 126, e2021JD034826.

Kemper, K.A., House Jr,, J., 1990. A DSC and IR study of the phase transition in anhydrous sodium acetate. Thermochim. Acta 170, 253–261.

Kerminen, V.M., Teinilä, K., Hillamo, R., Pakkanen, T., 1998. Substitution of chloride in sea-salt particles by inorganic and organic anions. J. Aero. Sci. 29, 929–942.

Laskin, A., Moffet, R.C., Gilles, M.K., Fast, J.D., Zaveri, R.A., Wang, B.B., et al., 2012. Tropospheric chemistry of internally mixed sea salt and organic particles: surprising reactivity of NaCl with weak organic acids. J. Geophys. Res. Atmos. 117, D15302.

Li, H.J., Zhu, T., Zhao, D.F., Zhang, Z.F., Chen, Z.M., 2010. Kinetics and mechanisms of heterogeneous reaction of NO_2 on $CaCO_3$ surfaces under dry and wet conditions. Atmos. Chem. Phys. 10, 463–474.

Li, J.Y., Gao, W.K., Cao, L.M., Xiao, Y., Zhang, Y.M., Zhao, S.M., et al., 2021. Significant changes in autumn and winter aerosol composition and sources in Beijing from 2012 to 2018: effects of clean air actions. Environ. Pollut. 268, 115855.

Li, R., Jia, X.H., Wang, F., Ren, Y., Wang, X., Zhang, H.H., et al., 2020. Heterogeneous reaction of NO_2 with hematite, goethite and magnetite: Implications for nitrate formation and iron solubility enhancement. Chemosphere 242, 125273.

Lian, H.Y., Pang, S.F., He, X., Yang, M., Ma, J.B., Zhang, Y.H., 2020. Heterogeneous reactions of isoprene and ozone on alpha-Al_2O_3: the suppression effect of relative humidity. Chemosphere 240, 124744.

Liu, C., Ma, Q.X., Liu, Y.C., Ma, J.Z., He, H., 2012. Synergistic reaction between SO_2 and NO_2 on mineral oxides: a potential formation pathway of sulfate aerosol. Phys. Chem. Chem. Phys. 14, 1668–1676.

Liu, W.J., He, X., Pang, S.F., Zhang, Y.H., 2017. Effect of relative humidity on O_3 and NO_2 oxidation of SO_2 on α-Al_2O_3 particles. Atmos. Environ. 167, 245–253.

Liu, Y.C., Han, C., Ma, J.Z., Bao, X.L., He, H., 2015. Influence of relative humidity on heterogeneous kinetics of NO_2 on kaolin and hematite. Phys. Chem. Chem. Phys. 17, 19424–19431.

Lu, K.D., Fuchs, H., Hofzumahaus, A., Tan, Z.F., Wang, H.C., Zhang, L., et al., 2019. Fast photochemistry in wintertime haze: consequences for pollution mitigation strategies. Environ. Sci. Technol. 53, 10676–10684.

Lv, X.J., Wang, Y., Cai, C., Pang, S.F., Ma, J.B., Zhang, Y.H., 2018. Investigation of gel formation and volatilization of acetate acid in magnesium acetate droplets by the optical tweezers. Spectrochim. Acta A Mol. Biomol. Spectrosc. 200, 179–185.

Ma, S.S., Yang, W., Zheng, C.M., Pang, S.F., Zhang, Y.H., 2019. Subsecond measurements on aerosols: from hygroscopic growth factors to efflorescence kinetics. Atmos. Environ. 210, 177–185.

Noma, H., Miwa, Y., Yokoyama, I., Machida, K., 1991. Infrared and Raman intensity parameters of sodium acetate and their intensity distributions. J. Mol. Struct. 242, 207–219.

Pang, H.W., Zhang, Q., Lu, X.H., Li, K.N., Chen, H., Chen, J.M., et al., 2019. Nitrite-mediated photooxidation of vanillin in the atmospheric aqueous phase. Environ. Sci. Technol. 53, 14253–14263.

Peng, C.G., Chan, C.K., 2001. The water cycles of water-soluble organic salts of atmospheric importance. Atmos. Environ. 35, 1183–1192.

Ray, A.K., Davis, E.J., Ravindran, P., 1979. Determination of ultra-low vapor pressures by submicron droplet evaporation. J. Chem. Phys. 71, 582–587.

Sun, W.W., Wang, D.F., Yao, L., Fu, H.B., Fu, Q.Y., Wang, H.L., et al., 2019. Chemistry-triggered events of $PM_{2.5}$ explosive growth during late autumn and winter in Shanghai. China. Environ. Pollut. 254, 112864.

Tan, F., Jing, B., Tong, S.R., Ge, M.F., 2017. The effects of coexisting Na_2SO_4 on heterogeneous uptake of NO_2 on $CaCO_3$ particles at various RHs. Sci. Total Environ. 586, 930–938.

Tan, F., Tong, S.R., Jing, B., Hou, S.Q., Liu, Q.F., Li, K., et al., 2016. Heterogeneous reactions of NO_2 with $CaCO_3$–$(NH_4)_2SO_4$ mixtures at different relative humidities. Atmos. Chem. Phys. 16, 8081–8093.

Tian, M., Wang, H.B., Chen, Y., Yang, F.M., Zhang, X.H., Zou, Q., et al., 2016. Characteristics of aerosol pollution during heavy haze events in Suzhou, China. Atmos. Chem. Phys. 16, 7357–7371.

Tsai, Y.I., Sopajaree, K., Chotruksa, A., Wu, H.C., Kuo, S.C., 2013. Source indicators of biomass burning associated with inorganic salts and carboxylates in dry season ambient aerosol in Chiang Mai Basin, Thailand. Atmos. Environ. 78, 93–104.

Villena, G., Kleffmann, J., 2022. A source for the continuous generation of pure and quantifiable HONO mixtures. Atmos. Meas. Technol. 15, 627–637.

Wang, N., Cai, C., He, X., Pang, S.F., Zhang, Y.H., 2018. Vacuum FTIR study on the hygroscopicity of magnesium acetate aerosols. Spectrochim. Acta. A Mol. Biomol. Spectrosc. 192, 420–426.

Wang, T., Liu, Y.Y., Deng, Y., Cheng, H.Y., Yang, Y., Zhang, L.W., 2021. Photochemical reaction of NO_2 on photoactive mineral dust: mechanism and irradiation intensity dependence. J. Photochem. Photobio. A 416, 113319.

Wilmshurst, K., 1955. Vibrational assignment for sodium acetate. J. Chem. Phys. 23, 2463.

Wu, C., Zhang, S., Wang, G.H., Lv, S.J., Li, D.P., Liu, L., et al., 2020. Efficient heterogeneous formation of ammonium nitrate on the saline mineral particle surface in the atmosphere of east Asia during dust storm periods. Environ. Sci. Technol. 54, 15622–15630.

Wu, L.Y., Tong, S.R., Ge, M.F., 2013. Heterogeneous reaction of NO_2 on Al_2O_3: the effect of temperature on the nitrite and nitrate formation. J. Phys.Chem. A. 117, 4937–4944.

Wu, Z.J., Nowak, A., Poulain, L., Herrmann, H., Wiedensohler, A., 2011. Hygroscopic behavior of atmospherically relevant water-soluble carboxylic salts and their influence on the water uptake of ammonium sulfate. Atmos. Chem. Phys. 11, 12617–12626.

Xu, Q.C., Wang, S.X., Jiang, J.K., Bhattarai, N., Li, X.X., Chang, X., 2019. Nitrate dominates the chemical composition of $PM_{2.5}$ during haze event in Beijing. China. Sci. Total Environ. 689, 1293–1303.

Yabushita, A., Enami, S., Sakamoto, Y., Kawasaki, M., Hoffmann, M.R., Colussi, A.J., 2009. Anion-catalyzed dissolution of NO_2 on aqueous microdroplets. J. Phys. Chem. A 113, 4844–4848.

Yang, M., Ma, S.S., Ashraf, H., Pang, S.F., Zhang, Y.H., 2020. The influence of SO_2 as the Criegee intermediate scavenger on the heterogeneous oxidation of oleic acid. Atmos. Environ. 231, 117560.

Ye, C.X., Li, H.J., Zhu, T., Shang, J., Zhang, Z.F., Zhao, D.F., 2010. Heterogeneous reaction of NO_2 with sea salt particles. Sci. China Chem. 53, 2652–2656.

Yu, C., Wang, Z., Ma, Q.X., Xue, L.K., George, C., Wang, T., 2021. Measurement of heterogeneous uptake of NO_2 on inorganic particles, sea water and urban grime. J. Environ. Sci. 106, 124–135.

Zhou, W., Chen, C., Lei, L., Fu, P.Q., Sun, Y.L., 2021. Temporal variations and spatial distributions of gaseous and particulate air pollutants and their health risks during 2015–2019 in China. Environ. Pollut. 272, 116031.